Influence of atmospheric pressure plasma process parameters on the mechanical behavior of thermoplastic joints

Influence of atmospheric pressure plasma process parameters on the mechanical behaviour of thermoplastic joints

F. Moroni[1], F. Musiari[1]*, C. Sciancalepore[1,2], M. Messori[2,3]

[1]Università degli Studi di Parma, Dipartimento di Ingegneria e Architettura, Parco Area delle Scienze, 181/A, 43124 Parma, IT.

[2]Consorzio Interuniversitario Nazionale per la Scienza e la Tecnologia dei Materiali, INSTM, Via G. Giusti, 9, 50121, Firenze, IT

[3]Università degli Studi di Modena e Reggio Emilia, Dipartimento di Ingegneria, Via Pietro Vivarelli, 10, 41125 Modena, IT

The capability of the Atmospheric Pressure Plasma Treatment (APPT) to increase the shear strength of adhesively bonded Single Lap Joints (SLJ) realized with polymeric adherends was investigated, by exploring the different response obtainable by changing the surface-to-nozzle distance and the treatment speed and by considering an industrial application as target. Beyond APPT, abrasion and chemical treatments were also performed and considered as reference. Three thermoplastic resins were used as adherends: polypropylene (PP), polyethylene (PE) and polyamide 66 (PA66). In addition to the mechanical characterization, even the variation of the surface free energy associated with the different combinations of parameters employed for the APPT was evaluated by means of optical contact angle (OCA) measurements. Moreover, for some representative combinations of substrates and APPT parameters, the changes of the polymer chemical structure were assessed by means of infra-red spectroscopy (IR). Finally, the sensitivity of the mechanical behavior to the time between the treatment and the deposition of the adhesive was assessed. The results showed that, in a plasma treated joint, a decrease of the surface-to-nozzle distance assured however an increase of the shear strength with respect to the chemical treated samples, provided that the treatment speed was correspondingly risen up. The trend of the wettability with the process configuration appeared to be consistent with the one exhibited by the joint shear strength, while any apparent influence of the delay time was detectable within 24 hours, which allowed to assume that APPT represents a reliable pre-treatment technique for industrial applications.

Keywords: B. plasma, B. plastics, B. surface treatment, C. contact angles

*Corresponding author – e.mail: francesco.musiari@unipr.it, Tel: +39 0521906644

1 Introduction

The necessity of reduction of weight and therefore of cost of structures, which are more and more required by many industrial sectors, lead to an effort to optimize and rationalize even the methods employed to join different components and parts together. Adhesive bonding represents an excellent compromise between the requirement of increasing the lightness of the structures and the need to not excessively decrement their strength demands. The coupled use of adhesive bonding and polymeric materials is able to guarantee tremendous advantages with respect to the lightness requirements. The bottleneck, however, is represented by the need to adequately pre-treat the surfaces where the adhesive should be deposited, with the intent to increase their suitability for the adhesion and to assure, as much as possible, the quality of the joining process. Several treatments aimed at this target were developed, for both metallic and polymeric materials. This last one class of materials demonstrated to be more sensitive to some specific pre-treatments, namely electric corona discharge, chemical or flame oxidation, metal-ion treatment, application of primers and finally treatments involving the use of ionized inert gas [1]. In particular, the chemical action provided by an ionized gas on a surface is the operating principle of the Atmospheric Pressure Plasma Treatment (APPT). This method was successfully tested on substrates realized in different classes of materials [2-5] and it was confirmed, under specific conditions, to be an optimal strategy to increase the surface free energy of polymeric surfaces, whose low values represent one of the biggest issues in using polymers as adherend materials for adhesive bonding purposes. Many works addressed the issue of the application of APPT on this last class of materials. In [6] the effect of APPT on polypropylene and polyethylene terephthalate (PET) film surfaces was assessed with respect to both the increment of the surface free energy and to the increase of the adhesion strength, which was enhanced by the changes in topography and in chemical composition induced by the treatment. A similar approach was followed in [7] on polyethylene surfaces. In [8] the APPT was compared with mechanical abrasion and chemical primer application by assessing their effect on some polypropylene Single Lap shear Joints (SLJ): the mechanical abrasion led to adhesive detachment even before the performance of the tests, while the APPT combined with the application of a chemical primer was found to impart almost 3 times higher shear strength with respect to the pristine specimens values. The capability of APPT to enhance the polymer surface energy is due to the formation of bonds between the reactive species, induced by plasma discharge using atmospheric air, and the polymeric surface. Plasma surface treatment of different polymers results in the oxidation of the surface by the generation of particular functional groups. In fact, XPS measurements showed the presence of oxygen-containing functionalities such as alcohols, aldehydes, ketones and carboxylic acids on polyethylene [9, 10], polypropylene [11, 12] and

polyamide [13] surfaces after APPT. Moreover, during plasma surface modification, the C-C and C-H bonds are broken and free radicals are formed on the polymer surface. Free radicals can give rise to processes such as recombination, unsaturation, branching, and crosslinking [14].

Several authors attempted an optimization of the APPT process parameters in order to identify the combinations able to assure the best performance of the surfaces in terms of adhesion strength. For instance, in [15] and [16] the influence of a variation of some factors on the wettability and the mechanical properties of polyamide surfaces was investigated, while in [17] the focus was placed on polypropylene substrates. In this work, APPT parameters, surface-to-nozzle distance and treatment speed, already found to be the most influential parameters to be optimized in order to drive the effectiveness of the treatment [18, 19], were varied to evaluate the effect on the surface free energy of three thermoplastics, namely polypropylene (PP), polyethylene (PE) and polyamide 66 (PA66). The variation of the surface free energy associated to the different combinations of employed parameters was evaluated by means of optical contact angle (OCA) measurements. The changes of the polymer chemical structure and the presence of final oxidation products after APPT were assessed by Fourier Transform Infra-Red spectroscopy (FTIR) for some representative plasma treated polymeric substrates. The same materials were employed to produce the substrates of adhesively bonded SLJ and to test the sensitivity of the shear strength to the variation of the process parameters. All the tests were repeated also on sets of specimens undergoing other traditional pre-treatments, namely the mechanical abrasion and the application of a chemical primer. OCA and FTIR results were correlated to the mechanical behavior of SLJ. Finally, the considered treatments were compared even according to their capability to keep the shear strength untouched by the time between the execution of the treatment and the deposition of the adhesive. This issue was already addressed with particular reference to metallic substrates [20-21]. Even the change induced on the wettability of polymer surfaces by the decay time was studied. In [22] the wettability decrease of polypropylene surfaces pre-treated with different combinations of cold plasma process parameters was found to reach about 7% after 1 day from the treatment and nearly touched 30% after 10 days from the treatment. In this work, the effect of the decay time was evaluated in terms of strength, measured on joints assembled after being exposed up to 24 h to air after the treatment.

2 Experimental setup

2.1 Materials and geometry

The materials chosen for the experimental study carried out in this work were polyethylene (PE), polypropylene (PP) and polyamide 66 (PA66), since they are commonly used in several industrial fields (i.e. food, pharmaceutical, automotive). Polymers were supplied by Ensinger, Milano – IT.

More details concerning the mechanical properties and presence of additives for the three commercial polymers used, are given in Table 1.

Table 1 – Details of the polymers used for the joint production

Material	**Polyethylene (PE)**	**Polypropylene (PP)**	**Polyamide 66 (PA66)**
Supplier	Ensinger	Ensinger	Ensinger
Commercial Name	Tecafine PE 300 (PE-HD)	Tecafine PP-H (PP-H)	Tecamid 66 MO (PA 66)
Colour	Black	Grey	Black
Modulus of Elasticity [MPa]	1100	1700	3200
Yield Stress [MPa]	23	33	83
Additives	< 2 w/w % (Black Pigment)	< 2 w/w % (Grey Pigment and nucleating additives for crystallization)	< 2 w/w % (Black Pigment and Molybdenum bisulphite)

Teroson 9399 was used as adhesive. It is a commercial two components adhesive based on silane-modified polymers; it cures at room temperature within 24h after mixing. It is widely used for elastic bonding in several industrial fields, especially to connect metals and polymers. It is available in two different colours, black and grey (due to availability of the supplier, the black one was used for PE and PP, while the grey one was used for PA66). The supplier recommends the use of primer in order to ensure a reliable adhesion with polymers. In particular, Teroson PP 33 primer and Teroson SB 450 primer (both supplied by Henkel) were suggested for PE/PP and PA66 respectively.

The SLJ geometry was selected in order to verify the influence of the plasma treatment on the adhesion strength. For the test implementation, ASTM D 3163 [23] was taken as reference. The adopted joint geometry is schematically shown in Figure 1. The substrates thickness value (t_S) depended on the substrate material due to supplier limitation: the specific values are reported in Table 2 for each material. Joints were assembled in a specifically designed jig, in order to maintain a good control on the overlap length (L) and on the adhesive thickness (t_A).

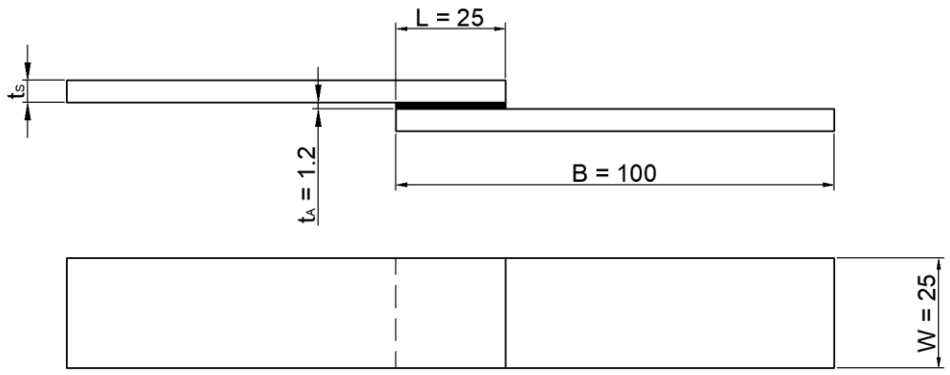

Figure 1 – Joint Geometry (dimension in mm)

Table 2 – Substrate Thickness for the three different substrates

Material	**PE**	**PP**	**PA66**
Substrate Thickness, t_S [mm]	4.0	4.0	6.6

2.2 Surface Treatments

Three different surface treatments were considered:

- Abrasion: as suggested by ASTM D 2093 - 03 [24] the surfaces were abraded with an Aluminum Oxide, 320 grit sand paper (free of waxes, lubricants or other contaminants), until no evidence of surface glossy was visible. Later the surfaces were wiped with a clean cloth and degreased with Henkel 7063 cleaner.
- Primer: the primer was applied to the surfaces to be bonded by means of a clean cloth. The joints were then assembled after approximately 25/30 minutes from the primer application. Following the adhesives supplier recommendation, Teroson PP 33 was used for PE and PP, while Teroson SB 450 was used for PA66.
- Plasma: the plasma treatment was carried out using an Atmospheric Plasma System, PlasmaBeam supplied by Diener. The machine is equipped with a 300 W generator and worked with air as both process and cooling gasses.

  The speed of the treatment (V) and the distance between the nozzle and the surface to be treated (D) are considered as process parameters (Figure 2) and varied in the ranges 30-400

mm/s and 5-20 mm, respectively. In order to cover the entire bonded surfaces, the treatment was performed along parallel lines: the distance between two adjacent lines were set to 4 mm (this value resulted the most appropriate from some preliminary tests). Once the plasma treatment was completed, the joints were assembled within 15 minutes. In order to understand the influence of the time between the execution of treatment and the deposition of adhesive, some specimens were also assembled 1, 2, 4, 16 or 24 hours after the treatment.

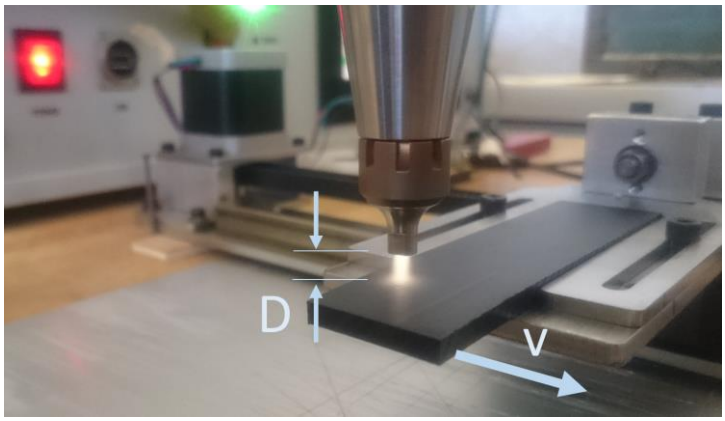

Figure 2 - Plasma treatment execution (identification of the two process parameters considered)

2.3 Surface free energy evaluation

Contact angles for different solid surfaces were evaluated by means of the contact angle meter OCA 20 (DataPhysics Instruments Gmbh, Filderstadt, Germany). Static contact angles were determined by the sessile drop method, on the basis of at least 5 measurements, with a drop volume of 1 µl using deionized water and high purity formamide (purity ≥99.5%, Sigma Aldrich, USA). The Owens-Wendt theory was used to calculate the polar (γ^p) and dispersive (γ^d) components of the surface free energy [25]. The surface free energy for each solid substrate was evaluated by means of Eq. (1).

$$\gamma = \gamma^p + \gamma^d \quad (1)$$

2.4 Surface infra-red spectroscopy

In order to obtain information on the changes in the chemical structure and composition of the plasma treated materials, for some representative specimens, infra-red spectra were acquired by means of an FT-IR Spectrum Two spectrophotometer (Perkin Helmer, USA) in the range 4000-400

cm^{-1}, before and after the plasma treatment. The spectra were recorded in attenuated total reflectance (ATR) mode, using a diamond window.

2.5 Mechanical characterization

Mechanical tests were carried out using an Instron 4400, electro-mechanical testing machine, equipped with a 30 kN load cell. Test speed was set to 3 mm/min, higher than the value of 1.2 mm/min suggested by ASTM D 3163 [23] in order to limit the time to failure of the specimens in 2 minutes and to reduce the effect of viscoelastic behaviour. Although the adhesive nominally cures in 24 hours at room temperature, with the aim of ensuring a complete adhesive polymerization, the specimens were tested at least 1 week after the joint manufacturing. At least four joints were assembled and tested for each treatment condition.

3 Results

3.1 PA66 specimens

Figure 3 presents the results of the mechanical tests for the specimens realized with PA66 substrates, while Figure 4 shows the appearance of the fracture surfaces for some noteworthy and representative cases for the same class of samples.

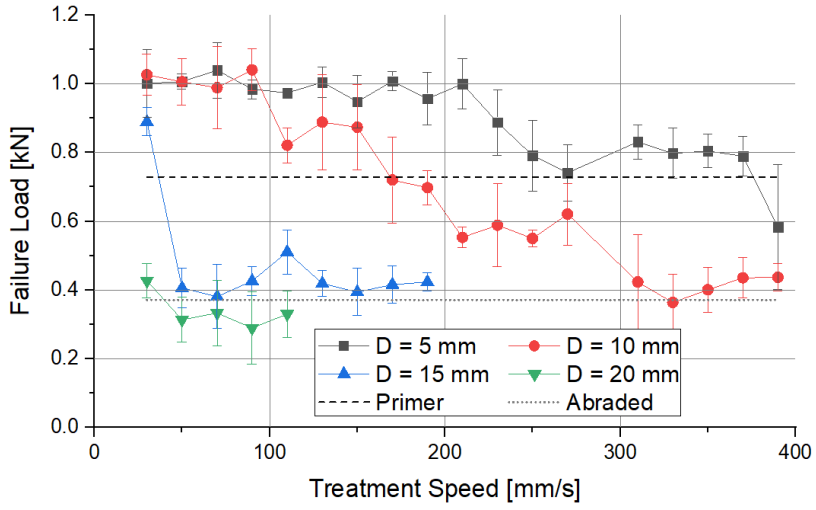

Figure 3 - Failure load of the PA66 SLJ as a function of the distance and the treatment speed

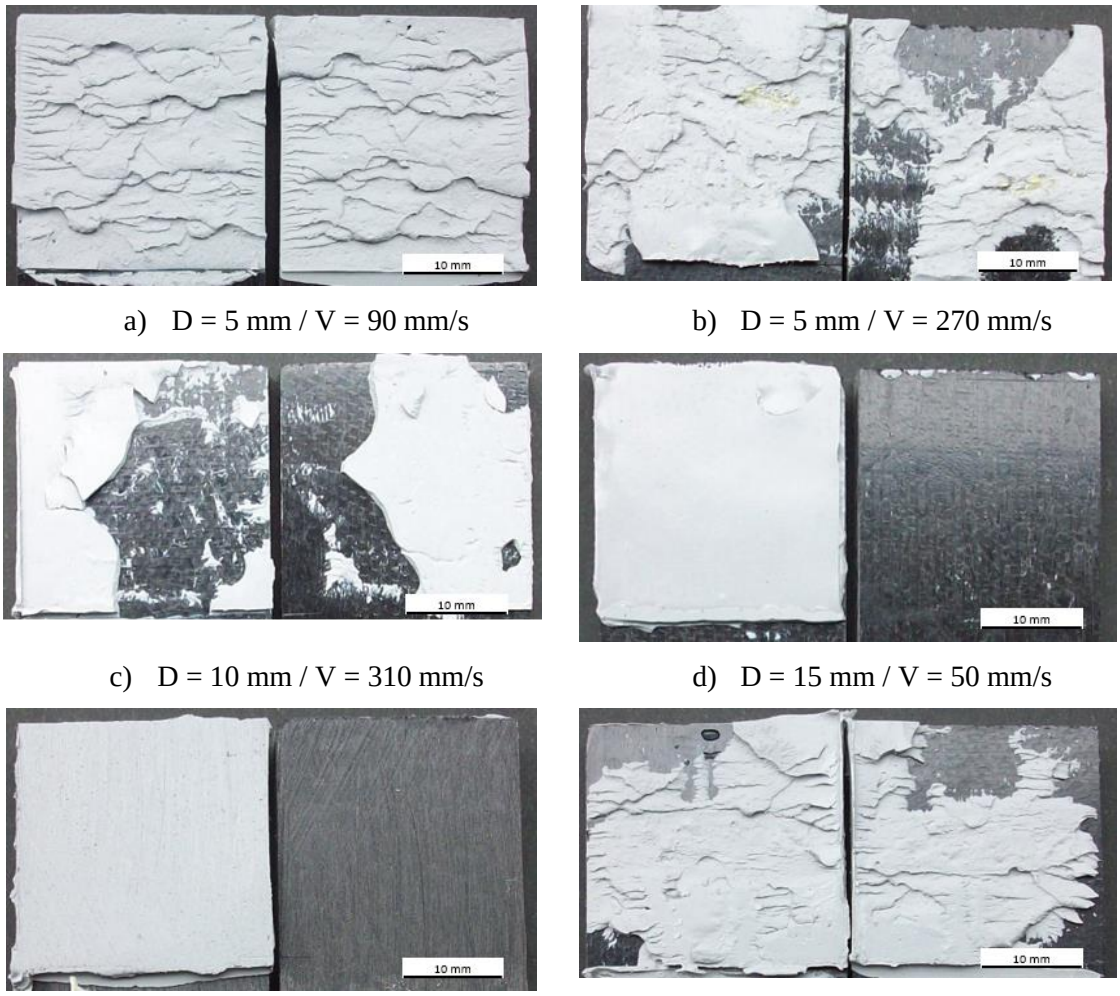

a) D = 5 mm / V = 90 mm/s

b) D = 5 mm / V = 270 mm/s

c) D = 10 mm / V = 310 mm/s

d) D = 15 mm / V = 50 mm/s

e) Abraded

f) Primer

Figure 4 - Example of the surface fracture of SLJ PA joints for different treatments (black substrates, grey adhesive)

In Figure 3, the differentiation occurring in the behavior of the different sets of specimens was evident. When D was equal to 20 mm, the lowest failure loads were recorded regardless from the level of speed of treatment employed, resulting in a mechanical response even worse than the one exhibited by the abraded specimens (with the exception of the plasma treated joints characterized by V = 30 mm/s). As D decreased to 15 mm, the failure load values appeared very close to the abraded result, except for the lowest value of V, which resulted in a failure load even higher than the one of the primer treated joints. A comparison between Figure 4 (d) and (e) revealed how the failure mode of the specimens with D = 15 mm and V higher than 30 mm/s appeared completely adhesive and therefore consistent with the one showed by the abraded joints. The mean failure load

curve belonging to the D = 10 mm set, instead, presented a wide extension, decreasing from about 1 kN for the lowest levels of speed, to overcome the primer treated samples result (approximately 0.75 kN, for V = 170 mm/s) and finally to touch the abraded result when V was equal to 330 mm/s. Figure 4 (c) showed that, for V = 310 mm/s, the specimens belonging to the D = 10 mm set presented a fracture surface characterized by a mixed adhesive/cohesive failure mode, but with a predominance of the interfacial mode, consistently with the appearance of the abraded fracture surface. Finally, the specimens pretreated with a surface-to-nozzle distance equal to 5 mm presented always higher failure loads than the primer treated samples result, until the speed V was kept below 390 mm/s. As the speed of treatment progressively increased and the failure load of the plasma treated joints belonging to this set got closer to the value associated with the primer treated samples which exhibited a mixed adhesive/cohesive fracture surface (Figure 4 (f)), the failure mode subsequently evolved from completely cohesive (Figure 4 (a)) to mixed adhesive/cohesive (Figure 4 (b)) behaviour. Figure 5 presents the amount of fracture surface interested in a cohesive failure, as it was assessed with the digital image processing, in function of the treatment speed for the PA66 case.

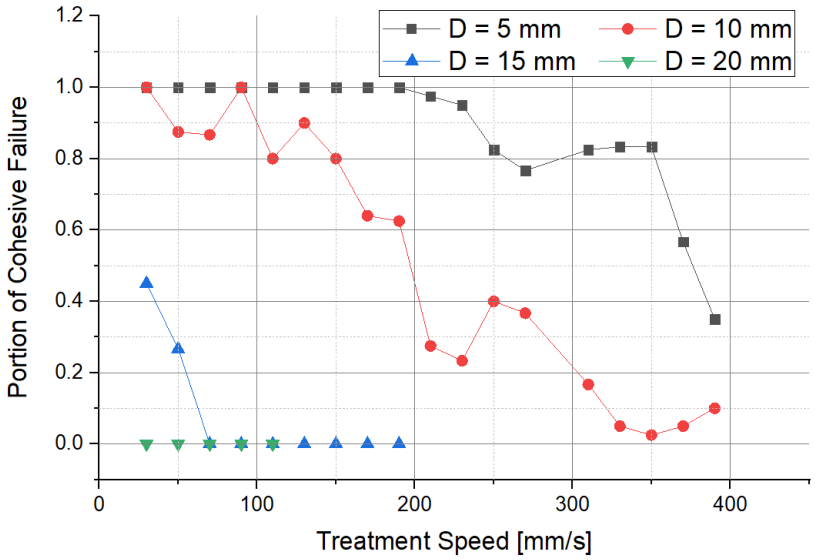

Figure 5 - Portion of cohesive failure of the PA66 SLJ as a function of the distance and of the treatment speed

The curves appeared consistent with the failure load results: the adhesive failure involved the D = 20 mm set regardless from the value of treatment speed and the D = 15 mm set for all the treatment speeds higher than 90 mm/s, while the D = 5 mm set exhibited a completely cohesive failure until 200 mm/s and finally the D = 10 mm set evolved from a completely cohesive to an almost adhesive

failure mode when the treatment speed increased from 30 mm/s to 390 mm/s. Figure 6 shows how the failure load of two different sets (the first with D = 5 mm and V = 210 mm/s, the second one with D = 10 mm and V = 130 mm/s) was not significantly affected by the delay time within the 24 hours.

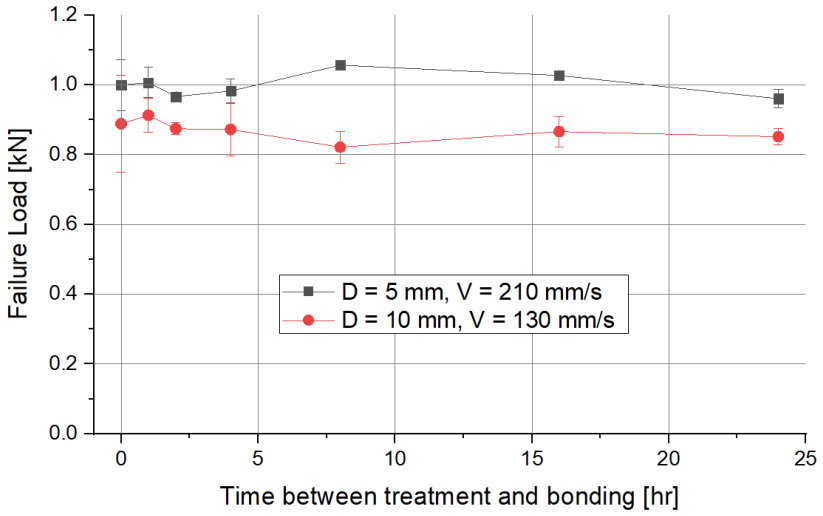

Figure 6 - Failure load of the PA66 SLJ as a function of the time between treatment and bonding

Figure 7 presents the results of the wettability measurements performed by the OCA on PA66 plasma treated surfaces. Figure 7(a) shows the surface free energy of PA66 samples as a function of the distance and the treatment speed, while the trend of its polar and dispersive components is plotted respectively in Figures 7 (b) and (c). Figure 7(a) reveals how the D = 15 mm set presented a significant decrease of the surface free energy with the treatment speed. This behavior was observed even in the failure load and the fraction of cohesive failure trends (Figure 5 and Figure 6) as a function of the plasma treatment speed.

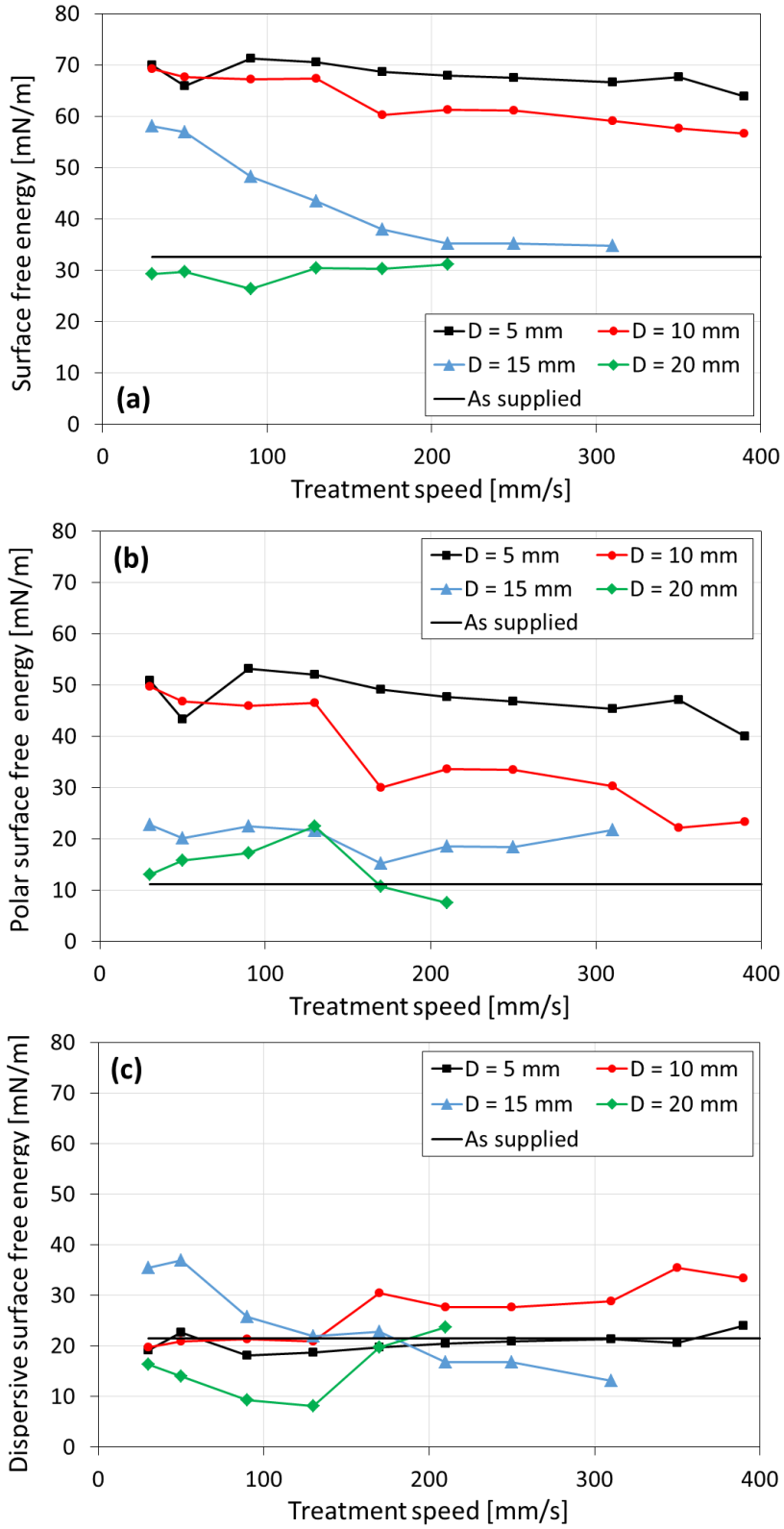

Figure 7 – Surface free energy (a), polar (b) and dispersive (c) components of surface free energy for PA66 samples as a function of the distance and the treatment speed.

Overall, an increase in surface energy, decreasing the distance and speed of treatment, was detected. The change in surface energy corresponded to the variation in surface wettability, determining the system transition from adhesive to cohesive failure. The enhanced wettability, consequent to the increased surface energy, could be correlated with the presence on the polymeric surface of carbonylic functional groups, due to atmospheric oxygen reaction with the amide groups present along the macromolecules during APPT, as evidenced by the IR spectra shown in Figure 8.

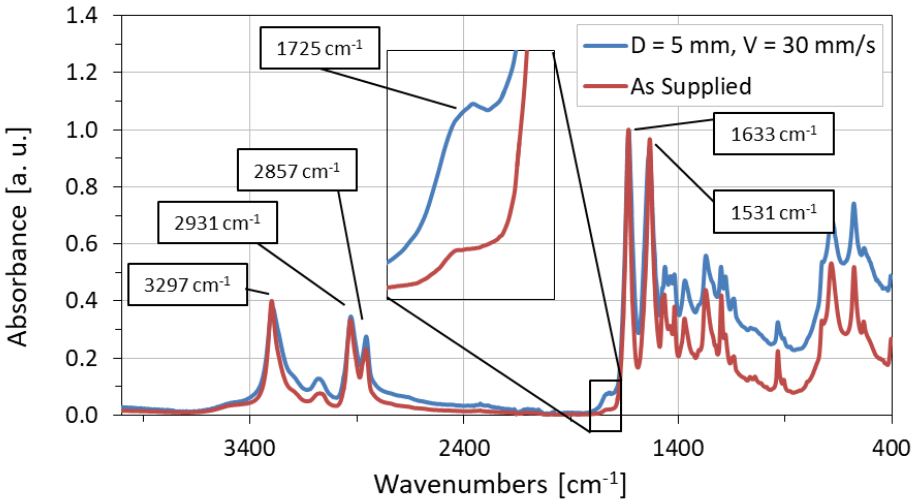

Figure 8 – IR spectra of the PA66 surface: "As supplied" (red line) and D = 5 mm, V = 3 mm/s (blue line) respectively, as representative samples. In the inset the resulting peak after APPT is shown. Characteristic peaks are labelled by the corresponding wavenumbers.

The FT-IR spectra of untreated and APPT PA66 samples exhibited the typical bands of PA66 at 3297, 2931 and 2857 cm^{-1}, attributable to NH_2 stretching, $-CH_2$ asymmetric and symmetric stretching vibrations, respectively. The strong intensity peaks of N-C=O stretching (amide I) and N-H bending (amide II) were identified at 1633 and 1531 cm^{-1} [26]. A peculiarity of the APPT PA66 samples was the presence of a new weak peak at about 1725 cm^{-1} (inset of Figure 8). This peak could be related to the C=O stretching vibration of carbonyl group, formed by reactive oxygen species during APPT [27, 28, 29].

3.2 PP specimens

Moving to consider the PP substrates case, it was worth to notice from Figure 9 that the failure load of the plasma joints pretreated with the lowest value of treatment speed (V = 30 mm/s) was not affected by the value of the surface-to-nozzle distance employed for the treatment. Then, the two sets with the higher values of D (D = 20 mm and D = 15 mm) progressively decreased below that value: the first set approached the failure load value of the abraded specimens (0.2 kN) for treatment speeds higher than 110 mm/s, while the second one reached the failure load of the primer treated sample for treatment rates greater than 90 mm/s.

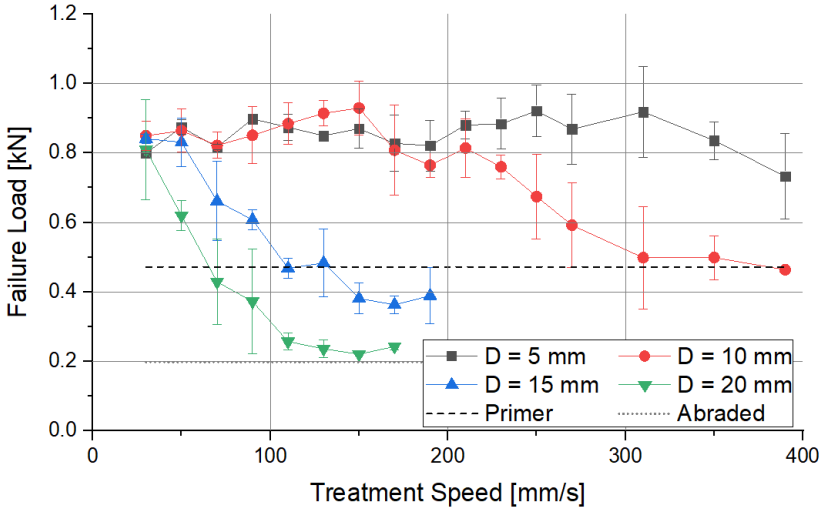

Figure 9 – Failure load of the PP SLJ as a function of the distance and the treatment speed

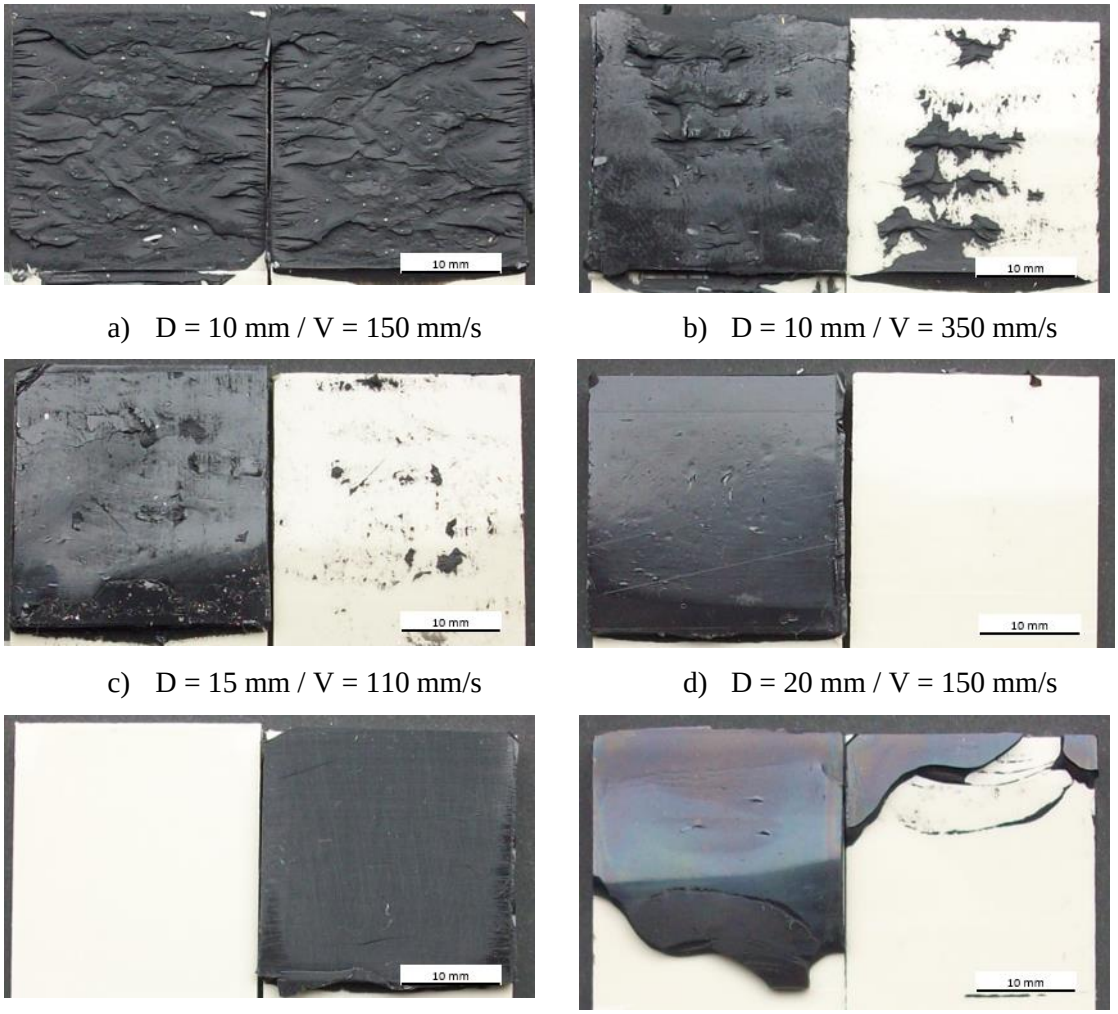

a) D = 10 mm / V = 150 mm/s

b) D = 10 mm / V = 350 mm/s

c) D = 15 mm / V = 110 mm/s

d) D = 20 mm / V = 150 mm/s

e) Abraded

f) Primer

Figure 10 – Example of the surface fracture of SLJ PP joints for different treatments. (grey substrates, black adhesive)

Figure 10 (c) and (d), respectively, depict the fracture surfaces of some D = 15 mm and D = 20 mm samples, pre-treated with levels of treatment speed high enough to make their locus of failure be placed at the substrate/adhesive interface, as in the abraded case (Figure 10 (e)). The evolution of the D = 10 mm curve appeared similar to the one described for the PA66 class of specimens, although even for very high rate values the failure load resulted still much above the abraded result. The threshold value over which the failure load of the plasma joints decreased, for this set, was found in the range between 210 mm/s and 230 mm/s. As a consequence, comparing the fracture surfaces associated with two samples of this set, the first one produced with a treatment speed lower

than the threshold (V = 150 mm/s), the second one with a treatment speed higher than the threshold (V = 350 mm/s), a remarkable switch of the locus of failure from within the adhesive to the substrate/adhesive interface was apparent (Figure 10 (a) and Figure 10 (b), respectively). The set with D = 5 mm presented failure loads always higher than the primer treated joints result, for the entire range of considered speeds.

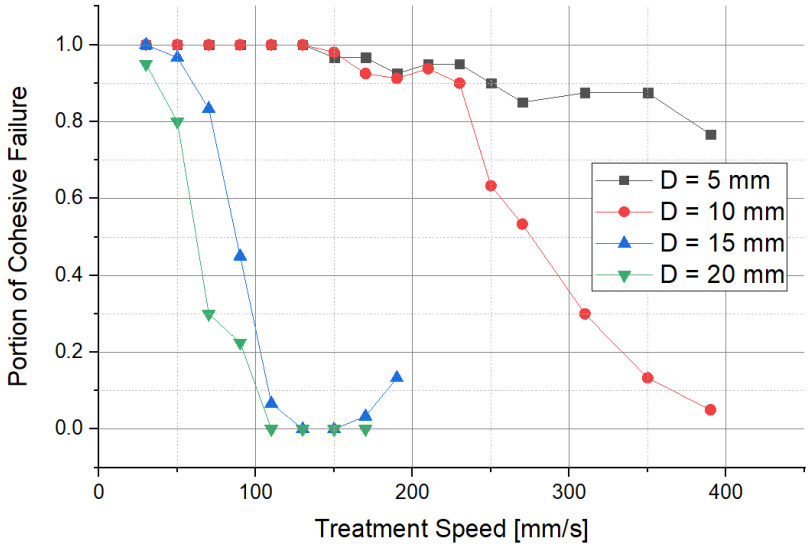

Figure 11 – Portion of cohesive failure of the PP SLJ as a function of the distance and of the treatment speed

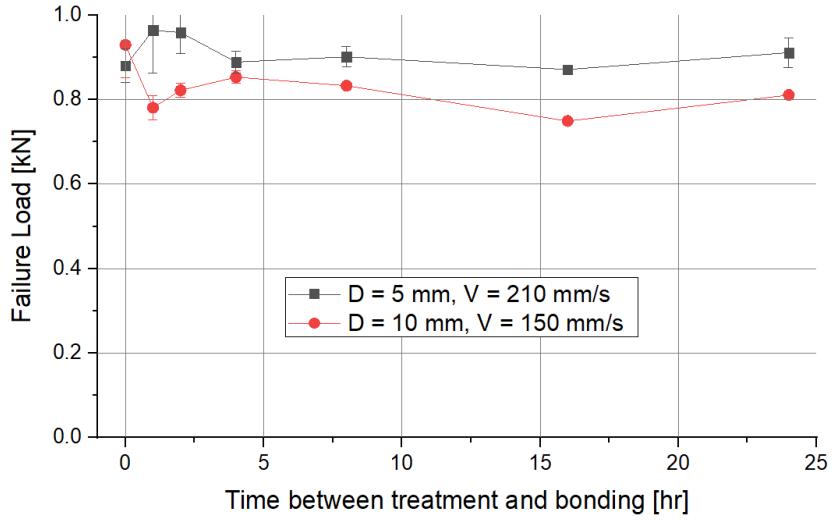

Figure 12 – Failure load of the PP SLJ as a function of the time between treatment and bonding

From Figure 11, the failure mode of the specimens associated with D = 20 mm and D = 15 mm sets, unlike the PA66 case, resulted predominantly cohesive for very low values of treatment speed (V < 50 - 70 mm/s). The failure occurring in the specimens treated with D = 10 mm resulted cohesive until V (rate) reached 230 mm/s, while the D = 5 mm set was characterized by the predominance of the cohesive failure mode for every tested level of treatment speed. Only for the highest treatment speeds (V > 300 mm/s) small portions of adhesive failure were observed. Figure 12 depicts the influence of the passing of time between treatment and bonding on the mechanical behavior of two different sets pre-treated using different combinations of plasma parameters: the one processed with D = 5 mm and V = 210 mm/s seemed, similarly to what was noticed for the joints with PA66 substrates, to not have any significant influence of the passing of time, while the set with D = 10 mm and V = 150 mm/s presented a slight decrease of the failure load with time, from beyond to below the results belonging to the other set.

Figure 13 (a) shows the surface free energy of PP samples as a function of the distance and the treatment speed, while the trend of its polar and dispersive components is plotted respectively in Figure 13 (b) and (c). With reference to the wettability measurements on the PP substrates, depicted in Figure 13 (a), the D = 5 mm set appeared the most peculiar, with the surface free energy starting from a value analogue to the untreated one (probably caused by the high amount of melted material generated at low treatment speeds) and increasing to values greater than almost 200% the initial result and finally decreasing for very high treatment speeds.

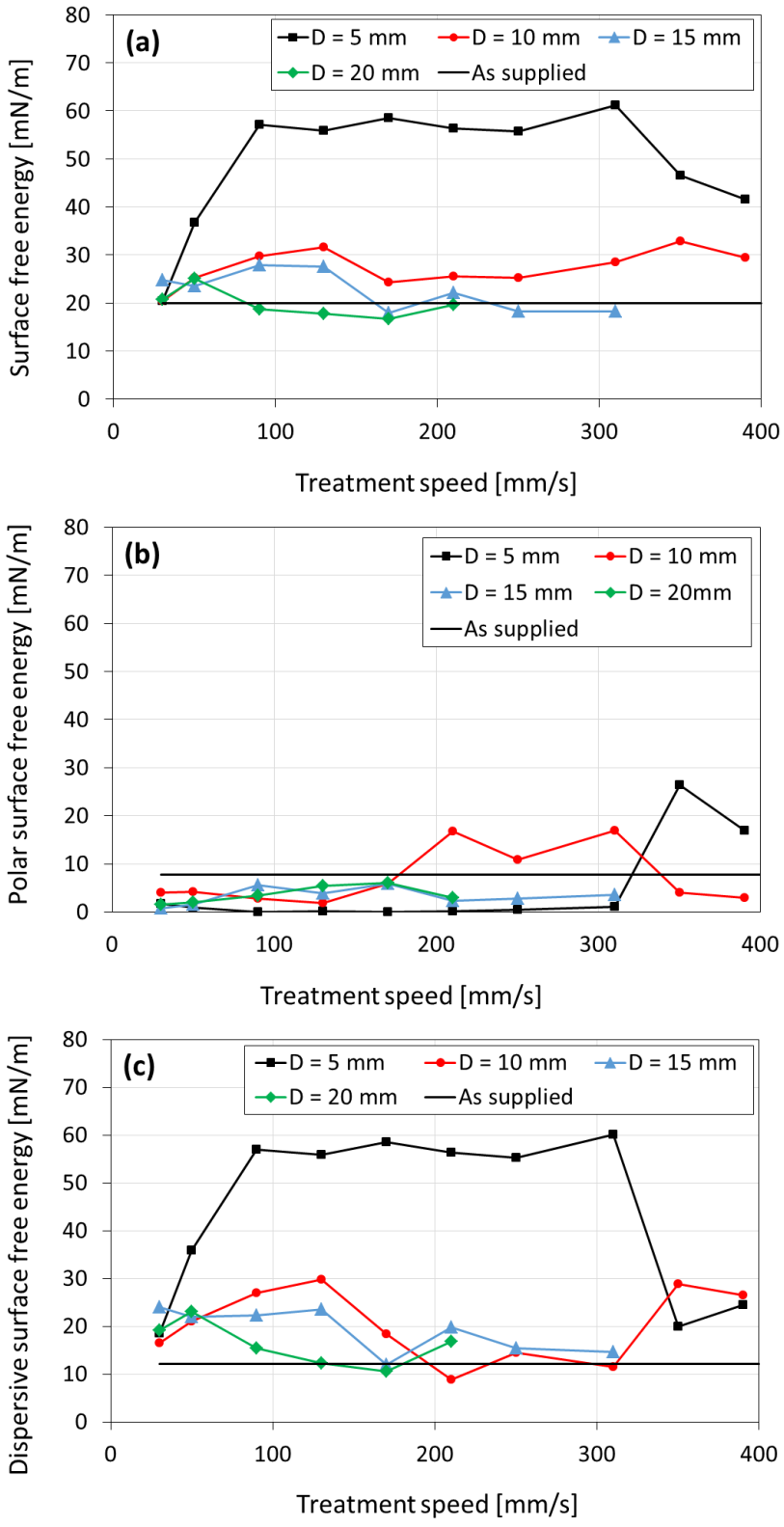

Figure 13 – Surface Free Energy (a), polar (b) and dispersive (c) components of Surface free Energy for the PP sample as a function of the distance and the treatment speed.

As general behaviour, however, surface energy values tended to decrease as the plasma treatment distance increased,remaining very close to values found for the untreated sample. In order to investigate the chemical structure variation introduced on the PP surface by plasma treatment, FT-IR analysis was performed on the untreated and some representative APPT PP samples. The FT-IR spectra of "As supplied" (red line), D = 10 mm, V = 90 mm/s (green line) and D = 5 mm, V = 90 mm/s (blue line) are shown in Figure 14. All spectra showed four high peaks in the range 3000–2800 cm^{-1}: the peaks at 2950 and 2868 cm^{-1} could be attributed to -CH_3 asymmetric and symmetric stretching vibrations respectively, while the peaks at 2917 and 2838 cm^{-1} were assigned to -CH_2- asymmetric and symmetric stretching vibrations, respectively. The FTIR spectra also showed two intense peaks in the fingerprint region: the peak at 1455 cm^{-1} arose by the overlap of the -CH_3 asymmetric bending and -CH_2- scissoring vibrations, while the peak at 1376 cm^{-1} was due to -CH_3 symmetric bending vibration [26].

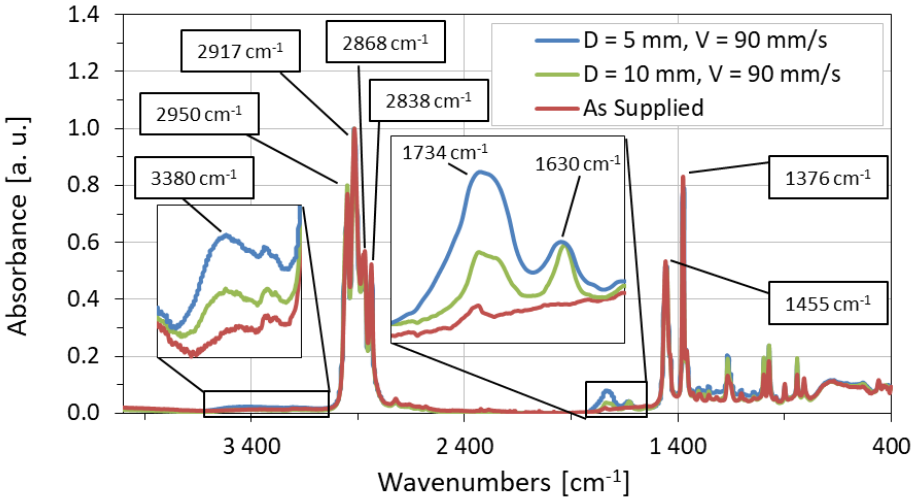

Figure 14 – IR spectra of the PP surface: "As Supplied" (red line), D = 10 mm, V = 90 mm/s (green line) and D = 5 mm, V = 90 mm/s (blue line) respectively, as representative sample. In the insets the resulting peaks after APPT are shown. Characteristic peaks are labelled by the corresponding wavenumbers.

Significant changes can be observed in the spectra of the plasma treated PP samples: a broad band (spiked at 3380 cm^{-1}) in the region 3200–3600 cm^{-1} was assigned to the O–H stretching vibration, and two new peaks were detected at 1734 and 1630 cm^{-1} (insets of Figure 14). The more pronounced peak at 1734 cm^{-1} was ascribed to the vibrations of C=O group, while the peak at 1630 cm^{-1} had a more uncertain attribution, although it had already been observed in other works and as a consequence of plasma treatments: reasonable hypotheses attributed this peak to possible unsaturated or nitrogen-containing functionalities [11, 30, 31, 32].

3.3 PE substrates

Finally, for what concerns the class of specimens produced with PE (Figure 15), even in this case the three sets characterized by D ranging from 5 mm to 15 mm and by V = 30 mm/s presented a failure load equal to 0.8 kN, followed by a decreasing trend which was similar to the one already described for the other two materials. While the failure in the abraded (Figure 16 (e)) and the primer treated (Figure 16 (f)) specimens resulted completely and predominantly interfacial, respectively, the fracture surface of the D = 5 mm specimens with V < 200 mm/s resulted affected by an almost completely cohesive failure, while it is worth noting that the failure mode in the D = 10 mm set progressively switched from cohesive to mixed and finally to wholly adhesive as the treatment speed increased. This trend is confirmed also looking at Figure 17 reporting the trends of the portions of cohesive failure with the treatment speed, for the different surface-to-nozzle values.

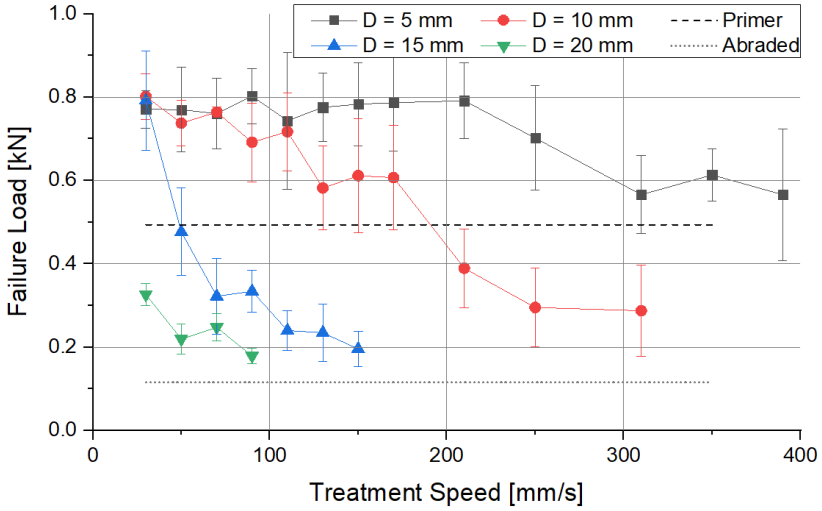

Figure 15 – Failure load of the PE SLJ as a function of the distance and the treatment speed

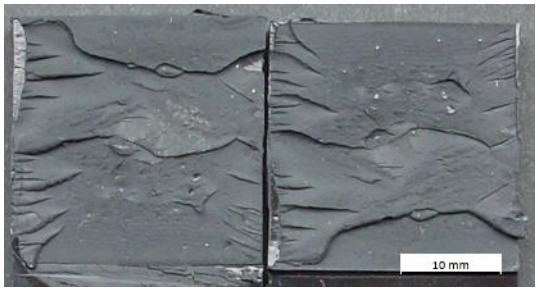

a) D = 5 mm / V = 170 mm/s

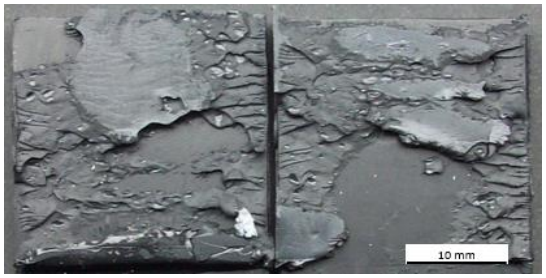

b) D = 10 mm / V = 130 mm/s

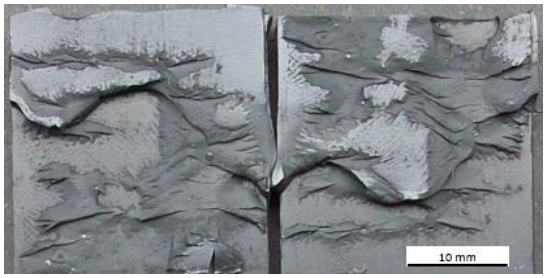

c) D = 5 mm / V = 310 mm/s

d) D = 10 mm / V = 250 mm/s

e) Abraded

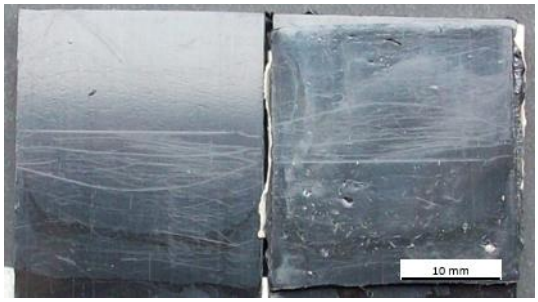

f) Primer

Figure 16 – Example of the surface fracture of SLJ PE joints for different treatments. (black substrates, black adhesive)

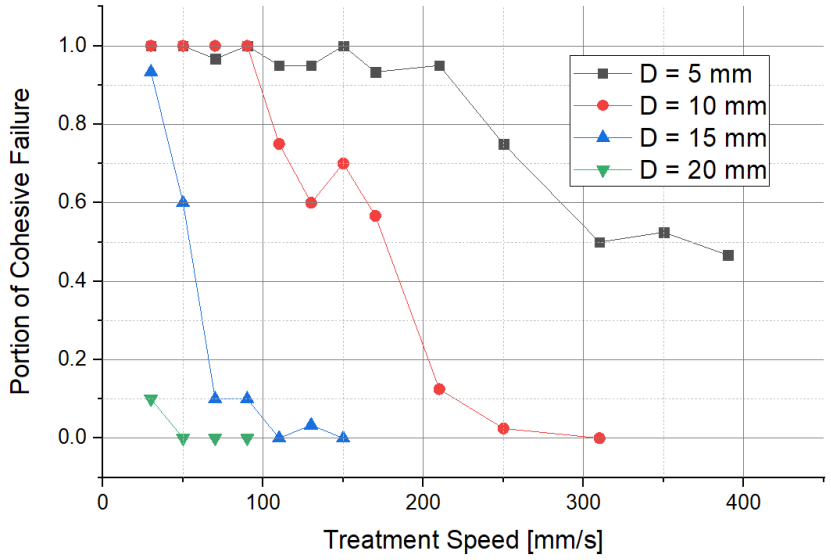

Figure 17 – Portion of cohesive failure of the PE SLJ as a function of the distance and of the treatment speed

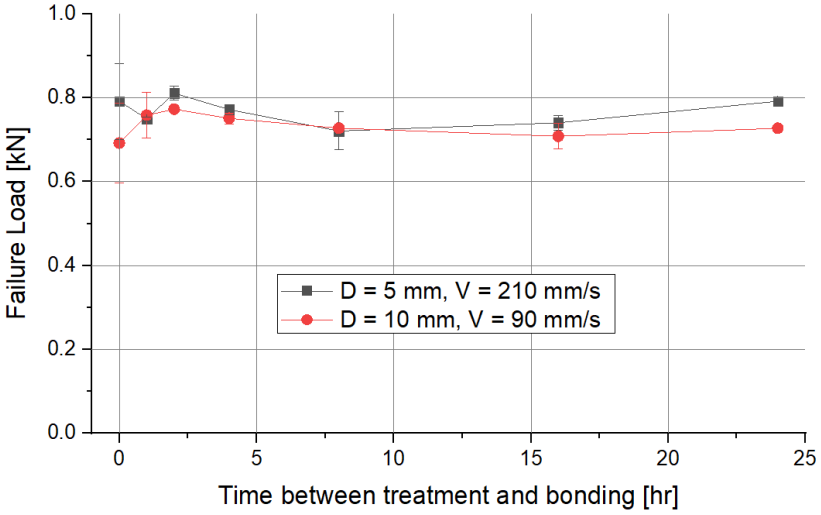

Figure 18 – Failure load of the PE SLJ as a function of the time between treatment and bonding

As shown in Figure 17, the independence of the failure mode of the D = 20 mm set (always adhesive) from the treatment speed was apparent, as well as the decrease of the portion of cohesive failure for the D = 15 mm set from 90% to 0% as V increased from 30 mm/s to 110 mm/s. For the D = 5 mm set the existence of a threshold in the treatment speed, whose overcoming determined the progressive increase of the percentage of adhesive area starting from a completely cohesive fracture surface, could be detected too, as in the PP case. Finally, by comparing the response of

different sets, as shown for instance in Figure 18, the substantial independence of the failure load from the time between the treatment and the bonding was confirmed even for the PE case.

Figure 19 (a) shows the surface free energy of PE samples as a function of the distance and the treatment speed, while the trend of its polar and dispersive components is plotted respectively in Figure 19 (b) and (c). Figure 19 (a) shows how the PE specimens characterized by the two lowest values of D were affected by a slight decrease of the surface free energy with the treatment speed. However, even if the surface free energy decrease for the D = 5 mm and D = 10 mm sets did not correspond to the relevant drop affecting the failure load and the failure mode of the corresponding specimens as the treatment speed increased, the trends of the wettability with the treatment speedwere quite consistent with the mechanical tests results, respectively

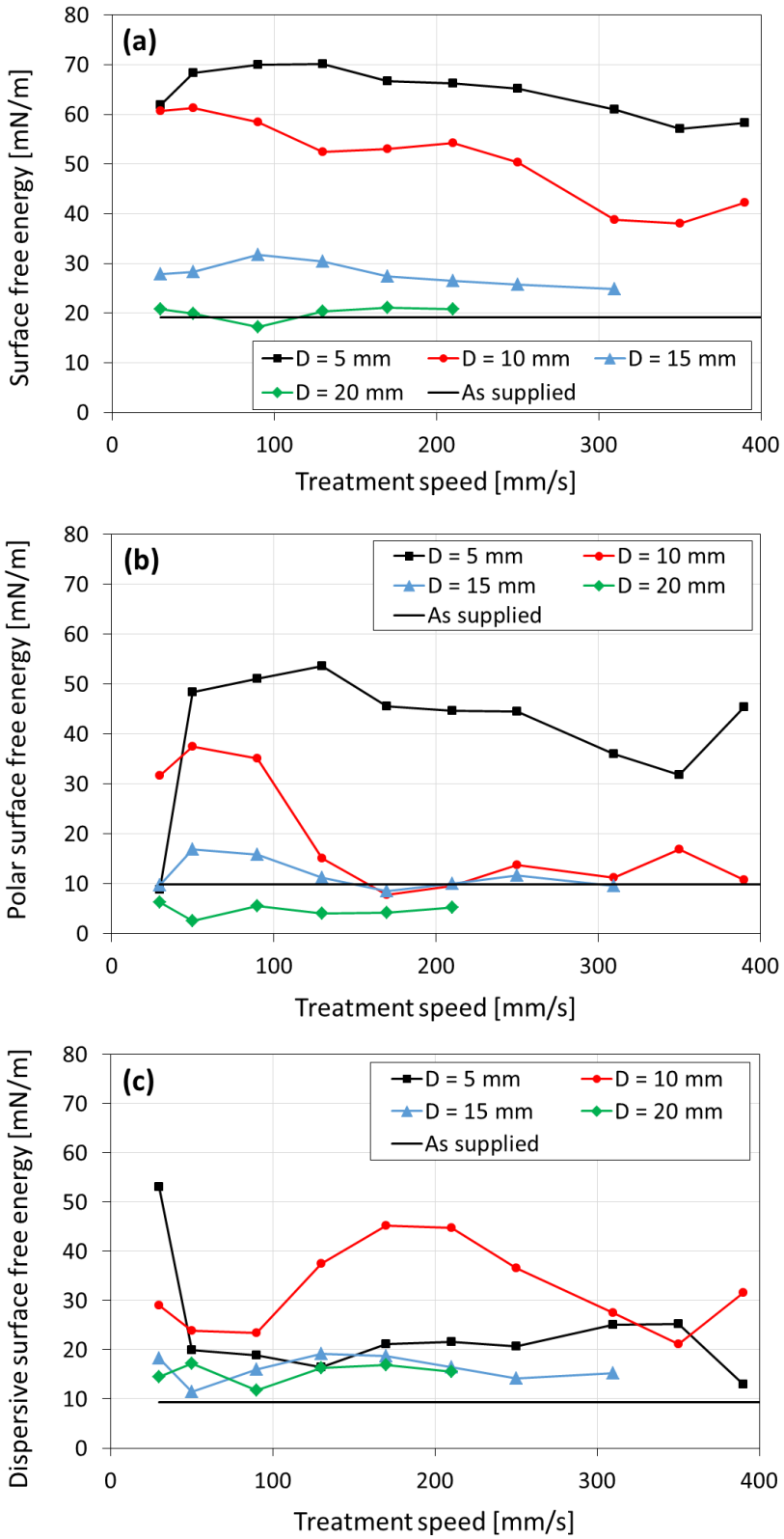

Figure 19 – Surface free energy (a), polar (b) and dispersive (c) components of surface free energy for the PE samples as a function of the distance and the treatment speed.

The observations on the variation of surface energy found correspondence in the surface chemical changes, detected by the FT-IR characterization.

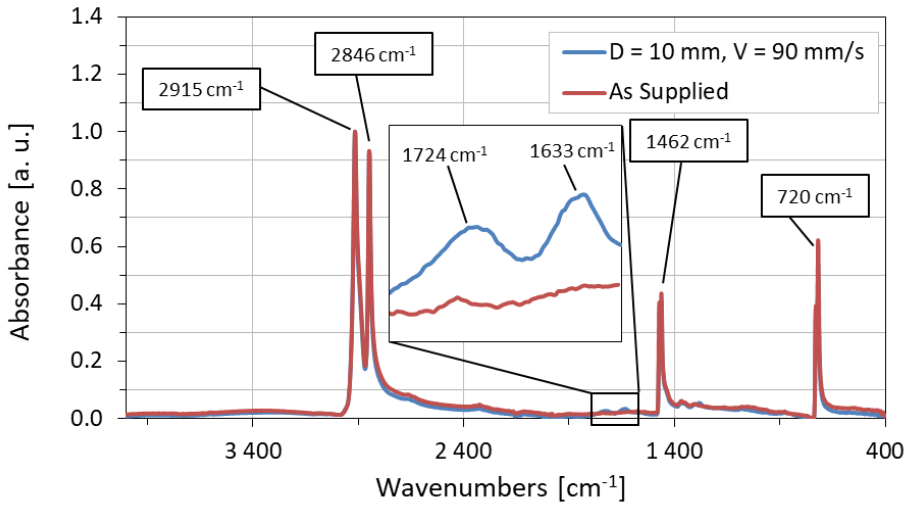

Figure 20 – IR spectra of the PE surface: "As supplied" (red line) and D = 10 mm, V = 90 mm/s (blue line) respectively, as representative samples. In the inset the resulting peaks after APPT are shown. Characteristic peaks are labelled by the corresponding wavenumbers.

Figure 20 shows the FTIR spectra of the untreated and D = 10 mm and V = 90 mm/s PE samples, as representative. Both spectra were characterized by two large absorption peaks at 2915 and 2846 cm^{-1} due to $–CH_2$ asymmetric and symmetric stretching vibrations, respectively. The spectra also showed two smaller absorption bands at 1462 and 720 cm^{-1}, attributed to $–CH_2$ – deformation and rocking vibrations, respectively [26]. The most remarkable difference after plasma treatment can be seen in the region 1800–1600 cm^{-1} (inset of Fig. 20). FTIR spectrum of the D = 10 mm, V = 90 mm/s sample showed a peak at 1724 cm^{-1}, arising after treatment, due to C=O stretching of probably different carbonyl-containing group species. Moreover, a second peak occurred at 1633 cm^{-1}, which could be attributed to the presence of C=C bonds stretching vibration [9,33].

3.4 Discussion

Although the results of the mechanical tests were slightly different according to the specific material employed to produce the substrates, a general trend of the failure load with respect to the values of the APPT process parameters was recognizable for each family of specimens. Even the ranking between the mechanical results associated with the samples treated with primer and with abrasion, respectively, was apparent, the second one results in every case significantly lower than

the first one by a factor ranging from approximately 2 to 5, depending from the substrate. With respect to the plasma treated joints, given a value of surface-to-nozzle distance (D), the recorded mean failure load decreased as the speed (V), used to perform the pre-treatment on the tested specimens, progressively increased, with some exceptions due to the data dispersion. Moreover, the lower surface-to-nozzle distance corresponds to the higher failure load, for the same treatment speed. For each value of D, a threshold value of speed, beyond which the failure load became equal or lower to the one associated with the joints undergoing the application of the chemical primer, was detectable. This threshold value was progressively lower as D increased. The observation of the fracture surfaces revealed an analogously consistent switch of the failure mode from mainly cohesive to prevalently interfacial as the failure load progressively decreased from beyond to below the strength of the specimens treated with the primer. Furthermore, as a general outcome, the trend of the failure load appeared consistent with the wettability measurements as resulting from OCA data. In general, for each considered material, the resulting surface free energy, according to the surface-to-nozzle distance, was consistent with the mechanical test results: the higher D, the lower is the corresponding surface free energy, which became fluctuating around the value associated with the untreated surfaces in the D = 20 mm case. Indeed, for high distances from sample surface the trend of the surface free energy seemed to be insensitive to the plasma treatment speed.

For the PA66 sample, the greatest influence on the total surface free energy was given by the polar fraction (Figure 7 (b) and (c)). This behavior can be mainly related to the presence of polar functional groups, such as carbonyl groups, due to plasma treatment. For the PP and PE samples, the dispersive part seemed to assume a greater importance in the statement of the final surface free energy (Figure 13 (b) and (c) and Figure 19 (b) and (c)). This result can be ascribed to the presence of highly energetic but apolar functionalities, such as alkenyl groups, detected on the PP and PE samples, arose after the plasma treatment,as detected by FTIR spectroscopy measurements.

In fact, from the FTIR analysis, absorptions referred to surface carbonyl groups, around 1730 cm^{-1}, were revealed in the spectra of all considered materials, in accordance with other works already published [9,11,27-33]. In the PE and PP samples the IR spectra showed the presence of another absorption peak around 1630 cm^{-1}, attributed to C=C stretching vibration, as result of plasma treatment [9,11,30,32,33]. As a matter of fact, plasma treatment of PE can also introduce vinyl groups on the polyolefin surface, as stated by Clouet and Shi [34], considering the dismutation reaction of the $-\dot{C}H-$ radicals, after H atom abstraction by oxygen atoms present in the discharge.

The presence of more reactive organic groups on the polymer surface caused the variation of the surface chemical environment with an increase of the surface free energy, depending on the specific

plasma treatment conditions. The incremented surface free energy tended to increase the wettability and therefore the adhesion properties of the polymer substrates.

4 Conclusions

In this work, several series of Single Lap Shear-Joints were produced using different polymeric materials (PA66, PP and PE, respectively) and by pre-treating them with different approaches. Some traditional mechanical (abrasion) and chemical (application of a primer) methods were tested and compared with the results gained with the APPT. In particular, two process parameters were selected in order to test the sensibility of the failure load of the cured joints to the specific configuration employed to perform the plasma treatment: the surface-to-nozzle distance and the treatment speed. The APPT was confirmed to be a successful process in order to increase the strength of polymeric adhesively bonded joints with respect to the abrasion and to the chemical treatment with a primer, when certain process parameters combinations were employed: the higher the nozzle-to-surface distance, the lower is the maximum treatment speed needed for keeping the failure load as high as possible. The measured portion of cohesive failure affecting the fracture surface of the specimens was consistent with the results of the mechanical tests, resulting in general in the occurrence of a complete adhesive failure when the failure load was similar to the one of the abraded joints, of a mixed adhesive/cohesive failure when the failure load was near to the value of the primer treated specimens and finally of a complete cohesive failure when the failure load was higher than the value found for the primer treated samples. The observed effect of the time between the treatment and the deposition of the adhesive on the mechanical response of the joints was negligible for the time range considered (up to 24 hours). The trend of the surface free energy with the treatment speed and the surface-to-nozzle distance was approximately the same of the failure load, although the variation ranges of the wettability resulted less marked than the ones associated with the switch of the failure mode and the decrease of the failure load occurring as the treatment speed increased. FTIR analyses provided qualitative information on plasma-modified polymer surfaces, detecting the presence of carbonyl groups and unsaturated functionalities, arising from APPT. These variations of the polymer chemical structure had the effect to increase the polymer surface energy, increasing consequently their wettability.

According to the obtained results, APPT has proven to be effective especially for low distances and low treatment speeds. These characteristics were consistent with wettability measurements and can be related to the observed mechanical behaviour.

Acknowledgments

This research was supported by the Italian Ministry for University and Research (MIUR), grant SIR RBSI146ZYJ.

References

1. Petrie EM. Handbook of adhesives and sealants. McGraw-Hill; 2000.
2. Saleema N, Gallant D. Atmospheric pressure plasma oxidation of AA6061-T6 aluminum alloy surface for strong and durable adhesive bonding applications. Appl Surf Sci 2013;282:98-104.
3. Shanahan MER, Bourgès-Monnier C. Effects of plasma treatment on the adhesion of an epoxy composite. Int J Adhes Adhes 1996;16:129-35.
4. Anagreh N, Dorn L, Bilke-Krause C. Low-pressure plasma pretreatment of polyphenylene sulphide (PPS) surfaces for adhesive bonding. Int J Adhes Adhes 2007;28:16-22.
5. Encinas N, Oakley BR, Belcher MA, Blohowiak KY, Dillingham RG, Abenojar J, Martinez MA. Surface modification of aircraft used composites for adhesive bonding. Int J Adhes Adhes 2014;50:157-63.
6. Navaneetha Pandiyaraj K, Selvarajan V, Deshmukh RR, Gao C. Adhesive properties of polypropylene (PP) film surfaces treated by DC glow discharge plasma. Vacuum 2009;83:332-39.
7. Choi DM, Park CK, Cho K, Park E. Adhesion improvement of epoxy resin/polyethylene joints by plasma treatment of polyethylene. Polymer 1997;25:6243-49.
8. Encinas N, Abenojar J, Martinez MA. Development of improved polypropylene adhesive bonding by abrasion and atmospheric plasma surface modifications. Int J Adhes Adhes 2012;33:1-6.
9. Li C, Liang CH, Huang C. Tailoring surface properties of polyethylene separator by low pressure 13.56MHz RF oxygen plasma glow discharge. Jap J App Phys 2016;55:01AF04-1-01AF04-6.
10. Foerch R, Kill G, Walzak MJ. Plasma surface modification of polyethylene: short-term vs. long-term plasma treatment. J Adhesion Sci Technol 1993;7:1077-1089
11. Morent R, De Geyter N, Leys C, Gengembre L, Payen E. Comparison between XPS- and FTIR-analysis of plasma-treated polypropylene film surfaces Surf. Interface Anal. 2008;40:597–600.
12. O'Hare LA, Leadley S and Parbhoo B. Surface physicochemistry of corona-discharge-treated polypropylene film. Surf. Interface Anal. 2002; 33: 335–342
13. Pappas D, Bujanda A, Demaree JD, Hirvonen JK, Kosik W, Jensen R, McKnight S. Surface modification of polyamide fibers and films using atmospheric plasmas. Surf Coat Tech 2006;201:4384–4388
14. Kusano Y. Atmospheric pressure plasma processing for polymer adhesion: a review. J. Adhesion 2014;90:755-777
15. Gao Z. Modification of surface properties of polyamide 6 films with atmospheric pressure plasma. Appl Surf Sci 2011;257:6068-72.
16. Mandolfino C, Lertora E, Gambaro C. Influence of cold plasma treatment parameters ion the mechanical properties of polyamide homogeneous bonded joints. Surf Coat Technol 2017;313:222-29.

17. Mandolfino C. Polypropylene surface modification by low pressure plasma to increase adhesive bonding: effect of process parameters. Surf Coat Technol 2019;366:331-37.

18. Noeske M, Degenhardt J, Strudthoff S, Lommatzsch U. Plasma jet treatment of five polymers at atmospheric pressure: surface modifications and the relevance for adhesion. Int J Adhes Adhes 2004;24:171-77.

19. Rodrìguez-Villanueva C, Encinas N, Abenojar J, Martìnez MA. Assessment of atmospheric plasma treatment cleaning effect on steel surfaces. Surf Coat Technol 2013;236:450-56.

20. Bònovà L, Zahoranovà A, Kovacik D, Zahoran M, Micusik M, Cernak M. Atmospheric pressure plasma treatment of flat aluminum surface. Appl Surf Sci 2015;331:79-86.

21. Tang S, Kwon O-H, Lu N, Choi H-S. Surface charateristics of AISI 304L stainless steel after an atmospheric pressure plasma treatment. Surf Coat Technol 2005;195:298-306.

22. Carrino L, Polini W, Sorrentino L. Ageing time of wettability on polypropylene surfaces processed by cold plasma. J Mater Process Technol 2004;153-154:519-525.

23. ASTM D 3163, Standard Test Method for Determining Strength of Adhesively Bonded Rigid Plastic Lap-Shear Joints in Shear by Tension Loading.

24. ASTM D 2093 – 03, Standard Practice for Preparation of Surfaces of Plastics Prior to Adhesive Bonding.

25. Owens DK, Wendt RC. Estimation of the Surface Free Energy of Polymers. J Appl Pol Sci 1969; 13: 1741-1747

26. Socrates G. Infrared and Raman Characteristic Group Frequencies – Tables and Charts (3rd edn). John Wiley & Sons; 2001.

27. Ribeiro AI, Senturk D, Silva KK, Modic M, Cvelbar U, Dinescu G, Mitu B, Nikiforov A, Leys C, Kuchakova I, De Vrieze M, Souto AP, Zille A. Antimicrobial efficacy of low concentration PVP-Silver nanoparticles deposited on DBD plasma-treated polyamide 6,6 fabric. Coatings 2019;9:581-595.

28. Zille A, Fernandes MM, Francesko A, Tzanov T, Fernandes M, Oliveira FR, Almeida L, Amorin T, Carneiro N, Esteves MF, Souto AP. Size and aging effect on antimicrobial efficiency of silver nanoparticles coated on polyamide fabrics activated by atmospheric DBD plasma. ACS Appl. Mater. Interfaces 2015;7:13731−13744.

29. Zhang W, Johnson L, Silva SRP, Lei MK. The effect of plasma modification on the sheet resistance of nylon fabrics coated with carbon nanotubes. Applied Surface Science 2012;258:8209– 8213.

30. Tran CTH, Craggs M, Smith LM, Stanley K, Kondyurin A, Bilek MM, McKenzie DR. Covalent linker-free immobilization of conjugatable oligonucleotides on polypropylene surfaces. RSC Adv 2016;6:83328–83336.

31. Dorai R, Kushner MJ. A model for plasma modification of polypropylene using atmospheric pressure discharges J. Phys. D: Appl. Phys. 2003;36:666–685.

32. Altuncu E, Üstel F, Esen SG, Karayel E. Infuence of oxygen and nitrogen plasma treatment on polypropyleme (PP) bumper surface J Achi Mat Manuf Eng 2016;77:18-23.

33. De Geyter N, Morent R, Leys C. Surface characterization of plasma-modified polyethylene by contact angle experiments and ATR-FTIR spectroscopy Surf. Interface Anal. 2008;40:608–611.

34. Clouet F, Shi MK. Interactions of Polymer Model Surfaces with Cold Plasmas: Hexatriacontane as a Model Molecule of High-Density Polyethylene and Octadecyl Octadecanoate as a Model of Polyester. 1. Degradation Rate versus Time and Power J. Appl. Polym. Sci. 1992;46:1955-1966.